AD_____

Award Number: W81XWH-08-1-0273

TITLE: Regularized Reconstruction of Dynamic Contrast-Enhanced MR Images for Evaluation of Breast Lesions

PRINCIPAL INVESTIGATOR: Kimberly A. Khalsa

CONTRACTING ORGANIZATION:

The University of Michigan

Ann Arbor, MI 48109-1274

REPORT DATE: January 2011

TYPE OF REPORT: Annual Summary

PREPARED FOR: U.S. Army Medical Research and Materiel Command
Fort Detrick, Maryland 21702-5012

DISTRIBUTION STATEMENT:

x Approved for public release; distribution unlimited

REPORT DOCUMENTATION PAGE

Form Approved
OMB No. 0704-0188

1. REPORT DATE *(DD-MM-YYYY)*	**2. REPORT TYPE**	**3. DATES COVERED** *(From - To)*
01-01-2011	Annual Summary	1 SEP 2010 - 31 DEC 2010

4. TITLE AND SUBTITLE
Regularized Reconstruction of Dynamic Contrast-Enhanced MR Images for Evaluation of Breast Lesions

5a. CONTRACT NUMBER

5b. GRANT NUMBER
W81XWH-08-1-0273

5c. PROGRAM ELEMENT NUMBER

6. AUTHOR(S)
Kimberly A. Khalsa
Jeffery A. Fessler

5d. PROJECT NUMBER

5e. TASK NUMBER

5f. WORK UNIT NUMBER

7. PERFORMING ORGANIZATION NAME(S) AND ADDRESS(ES)
The University of Michigan
Ann Arbor, MI 48109-1274

8. PERFORMING ORGANIZATION REPORT NUMBER

9. SPONSORING / MONITORING AGENCY NAME(S) AND ADDRESS(ES)
U.S. Army Medical Research and Materiel Command
Fort Detrick, MD 21702-5012

10. SPONSOR/MONITOR'S ACRONYM(S)

11. SPONSOR/MONITOR'S REPORT NUMBER(S)

12. DISTRIBUTION / AVAILABILITY STATEMENT
Approved for public release; distribution unlimited.

13. SUPPLEMENTARY NOTES

14. ABSTRACT

The overall goal of this project is to develop, implement, and evaluate methods for improving image quality in dynamic MR imaging. We focus specifically on dynamic contrast-enhanced (DCE) imaging of breast cancer patients. We explore reconstruction methods that use explicit temporal models in object space. Simulation and phantom studies have indicated that our algorithms produce quality reconstructed image sequences that exhibit favorable temporal resolution properties.

15. SUBJECT TERMS
Image reconstruction, dynamic contrast-enhanced MRI, breast MRI

16. SECURITY CLASSIFICATION OF:			**17. LIMITATION OF ABSTRACT**	**18. NUMBER OF PAGES**	**19a. NAME OF RESPONSIBLE PERSON**
a. REPORT	**b. ABSTRACT**	**c. THIS PAGE**			USAMRMC
U	U	U	UU	28	**19b. TELEPHONE NUMBER** *(include area code)*

Contents

1 Introduction

The overall goal of this project was to develop, implement, and evaluate methods for improving image quality in dynamic magnetic resonance imaging. We focused specifically on dynamic contrast-enhanced (DCE) imaging of breast cancer patients. The fundamental challenge in dynamic MRI is the tradeoff between spatial resolution and temporal resolution. In addressing this problem, most traditional dynamic acquisition methods and associated reconstruction methods have been based on operations in the data domain, known as k-space, implicitly assuming that the object varies smoothly in time. We explored an image reconstruction scheme based on an object domain model that does not attempt any k-space data recovery, but rather explicitly uses the assumption of temporal smoothness in the image domain to estimate the image sequence that best fits the available data. Our proposed method is called Temporal Regularization Use in Image Reconstruction (TRUIR), and is a penalized likelihood formulation that includes spatial and temporal regularization terms in addition to the data fidelity term. We incorporated parallel imaging, accelerated our algorithm, evaluated the effect of spatial and temporal regularization parameters on the resolution properties of reconstructed image sequences, and explored new phase encode sampling schemes that work well in conjunction with TRUIR.

2 Body

2.1 Reconstruction Model and Cost Function Design

Our proposed method for reconstructing DCE MR images is based on minimizing a three term image domain cost function. We call our method Temporal Regularization Use in Image Reconstruction (TRUIR). The first term in the cost function is a data fidelity term, which ensures that the image estimate is consistent with the measured data. The second and third terms in the cost function are weighted spatial and temporal penalty terms. We use these terms to incorporate our *a priori* knowledge about the object, namely that there is a certain smoothness expected in both space and time. The spatial regularizer penalizes large differences between neighboring pixels in space and the temporal regularizer penalizes large differences between neighboring pixels in time. There are regularization parameters α and β that determine the relative weighting within the cost function of the spatial and temporal regularization terms, respectively.

In the past decade the idea of using multiple receiver coils to simultaneously acquire MR data has been introduced and the practice is now widespread [1–3]. This is known as *parallel imaging* and, in general, reduces the required scan time. Therefore we deemed it important to incorporate parallel imaging into our methods and have done so.

In addition to the work discussed in the following sections, this year we have added many tools and functions to the group's code base, including the creation of a new data object to assist in TRUIR reconstructions. These additions will be available to fellow and future students and researchers, which will help ensure the long-term progress and viability of this

project.

2.2 Extension to Parallel Imaging

In the past decade the idea of simultaneously using multiple receiver coils to acquire MR data has been introduced and the practice is now widespread [1, 2]. This is known as *parallel imaging* and, in general, reduces the required scan time. Therefore we deemed it important to incorporate parallel imaging into our methods and have done so.

2.3 Algorithm Acceleration

A drawback of iterative reconstruction methods, compared to conventional methods, is increased computation time. For our proposed method, the most computationally expensive step in determining the image estimate is computing the gradient of the cost function. We were able to accelerate our computation by exploiting Toeplitz matrices in this step [4]. This acceleration technique has previously been investigated for use in static, field-corrected MR image reconstruction [5], but, to our knowledge, we are the first to apply it to dynamic MRI. For this study, the Toeplitz-modified algorithm was 1.7 times faster than the original algorithm.

2.4 Phase Encode Sampling Strategies

Because the data in most dynamic MR acquisitions is severely undersampled, the quality of most dynamic reconstruction schemes is heavily dependent on which k-space locations are sampled. We expect this to hold true for our TRUIR as well. We are in the process of exploring a variety of 2D phase encode (PE) sampling strategies to determine which have optimal temporal/ spatial resolution tradeoff for the TRUIR method.

The TRUIR formulation gives us some flexibility in terms of what we consider to be one time frame. An acquired set of data can be grouped in different ways to produce different reconstructed image sequences. That is, with a given amount of collected data, one can decide during post processing how many image frames one would like to reconstruct. For a given amount of data, reconstructing more frames means there is less data grouped in each frame. Traditionally, this would result in severe undersampling artifacts in the resultant image sequence, but because the TRUIR formulation includes an explicit temporal roughness penalty that enforces some connectivity between time frames, there is potential to have flexibility in the number of reconstructed frames (equivalently, frame rate), while maintaining image quality.

We compared three different phase encode sampling strategies. The first phase encode (PE) sampling scheme we studied is one that is currently in use for DCE MRI studies of the breast at the University of Michigan hospital, on a Philips 3T scanner. We refer to this as the Original Trajectory. It is an elliptically shuttered, partial Fourier acquisition, that is also undersampled by a factor of 2 in the SENSE direction, ky. The Original Trajectory is shown in Fig. 1, where the order in which the samples are acquired is indicated by the

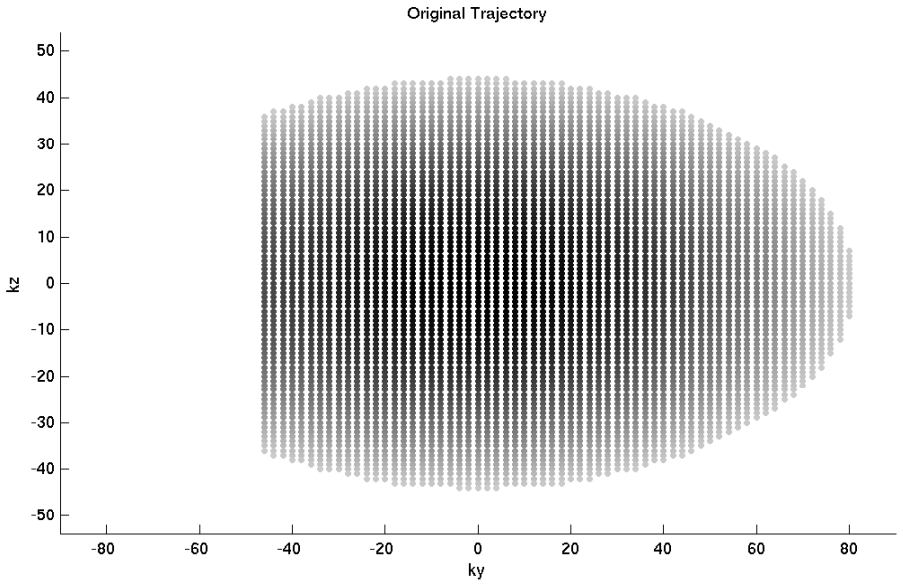

Figure 1: Original Trajectory. Dark circles represent PE locations that are sampled earlier in the acquisition, and light circles represent locations that are sampled later during acquisition. The Original Trajectory starts sampling near DC and works its way out, with the highest frequency sample locations being sampled latest in the acquisition.

darkness of the circle. The darker circles represent locations that are sampled earlier in the scan and lighter circles are locations that are sampled later, i.e., the overall sampling occurs from low frequency to high frequency. For the current reconstruction method used by the clinical scanner, the trajectory shown in Fig. 1 is collected for each reconstructed frame.

The low to high frequency ordering of the original PE acquisition means that if we break the data into 2 subframes, the first half-frame of PE locations will all be from lower spatial frequencies, while the second half-frame of data will all be from higher spatial frequencies. We would like the samples within each subframe to be more balanced than those from the Original Trajectory in terms of information content (i.e., each subframe contains samples from large range of frequencies), so that during post-processing, we have the option to increase the frame rate used for reconstruction. Towards this end, we developed two new PE sampling strategies, which are both composed of the same sample locations as the Original Trajectory, but acquired in a different order. We refer to these new PE sampling patterns as Reordered Trajectory 1 and Reordered Trajectory 2, and they are shown in Figs. 2 and 3, respectively. Both new trajectories are based on reordering schemes that aim to more uniformly distribute the samples in time, in terms of the samples' radial distance from the center of k-space. This feature is illustrated in Figure 4, which plots each sample location of the acquisition in terms of its radial distance from the center of k-space vs the time at which that that sample is acquired. In the plot for the Original Trajectory (top), the samples' increasing radial distance over time indicates the inside to out ordering of that trajectory, whereas the samples for both Reordered Trajectories clearly show more uniform distributions.

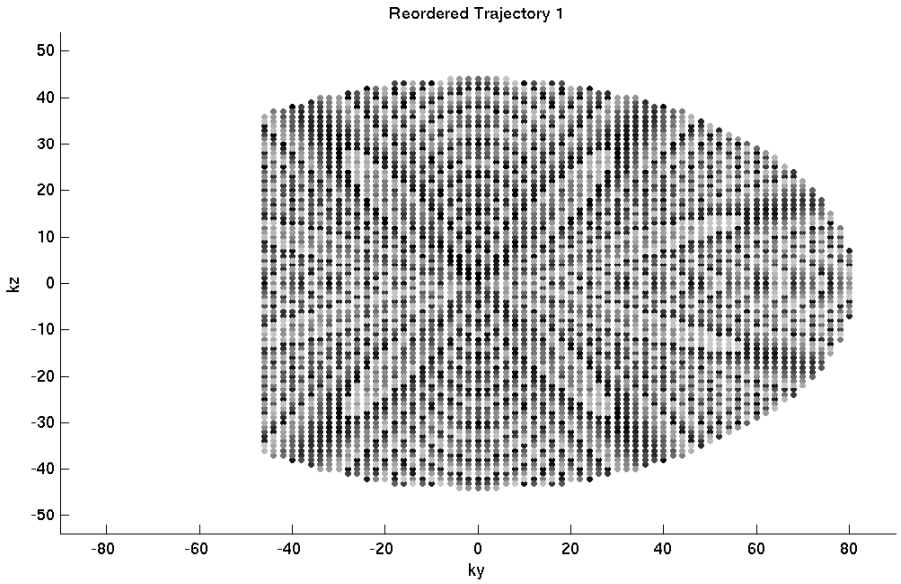

Figure 2: Reordered Trajectory 1.

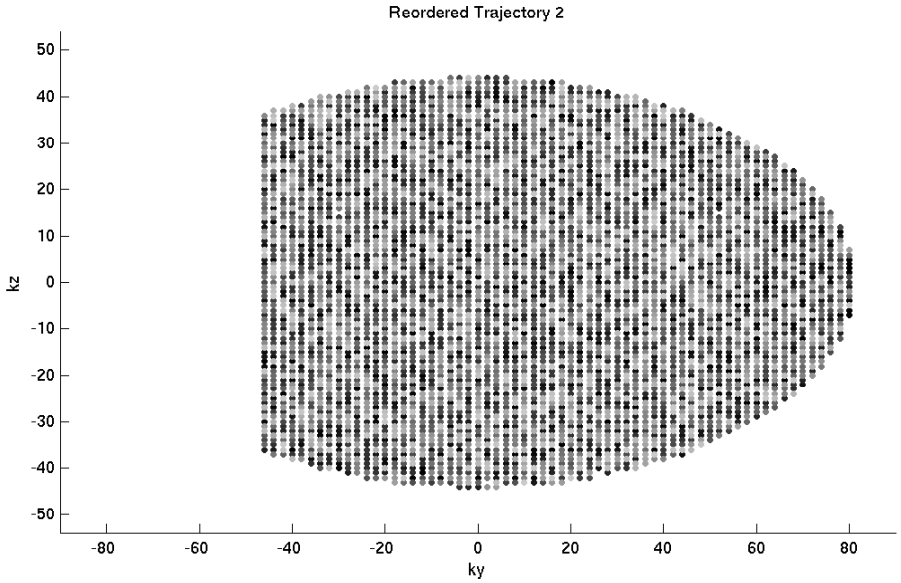

Figure 3: Reordered Trajectory 2.

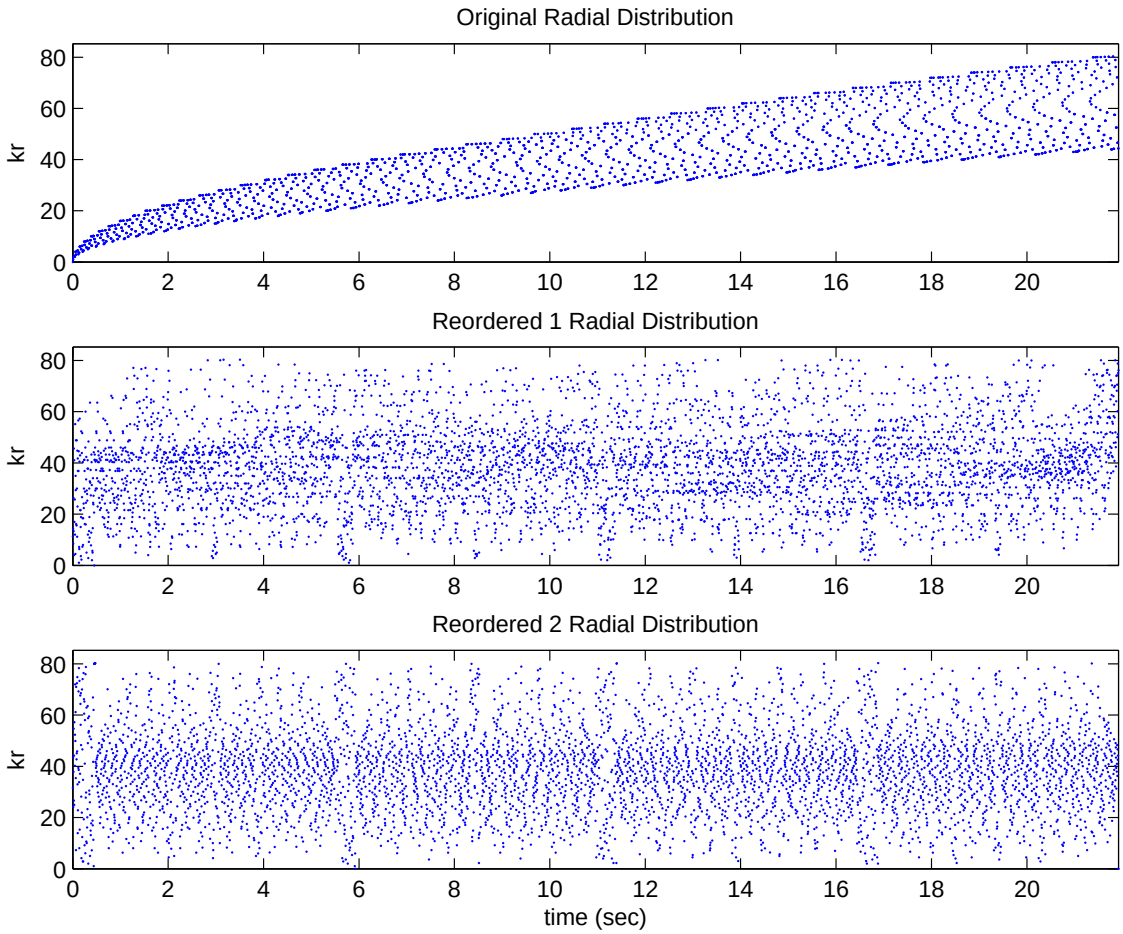

Figure 4: Radial distribution of sample locations over time. Original Trajectory (top), Reordered Trajectory 1 (middle), and Reordered Trajectory 2 (bottom). Both reordered trajectories show a more uniform distribution of sample locations over time, in terms of the samples' radial distance from the center of k-space (shown on the y-axis), than the Original Trajectory.

Figure 5 shows another comparison of the three PE trajectories. The PE locations sampled during the first half of a full acquisition are shown on the left, and for the second half of acquisition on the right, for each trajectory. During the first half of acquisition, the Original Trajectory covers only the low frequencies, while the first half of the Reordered Trajectories cover the entire range of frequencies of a full acquisition.

2.5 Regularization Parameters

A challenging aspect of any regularized formulation is choosing appropriate regularization terms, as well as determining the relative weights of these terms. In our formulation, the weighting of these terms is implemented with temporal and spatial regularization parameters, α and β. Regularization parameter choice can significantly influence the quality of the reconstructed images. For practical use of our reconstruction approach, one must understand how the regularization parameters α and β in the cost function affect the reconstructed images. For TRUIR reconstruction of dynamic image sequences, the temporal regularization parameter α is of particular importance. Essentially we want to use an α that is large enough to provide adequate "connectivity" between the frames, but small enough so that the reconstructed image sequence correctly reflects dynamic changes in the object.

We aimed to address the issue of regularization parameter choice by analyzing the resolution properties of the TRUIR method. To do this, we examined the local impulse response in space and time. Our initial evaluation looked at the spatial and temporal resolution of a TRUIR formulation for a single coil acquisition and found an expected relationship between β and spatial resolution, and α and temporal resolution [6]. Similar analysis of penalized-likelihood reconstruction for (static) tomography was presented in [7].

We then evaluated the effects of regularization parameter choice on the full TRUIR formulation, which includes parallel imaging. We have found that the analysis for the multi-coil case is significantly more complicated than the single coil case. We have not determined an analytical method for choosing the regularization parameters, but we have examined various aspects of the spatial point spread function (PSF) of a impulse that is static in time, and have found some measures that may be useful in selecting appropriate regularization parameter values.

We found that the variability in the full-width half-max (FWHM) of the spatial PSF may be one useful indicator for temporal regularization parameter selection (in some cases), and examining the energy in the tails of the spatial PSF may also be an effective method.

Figure 6 shows the spatial PSFs for TRUIR reconstructions using a range of temporal regularization parameters, $\log_2 \alpha = [-10 : 2 : 10]$. We evaluated the static impulse response of TRUIR reconstructions using $\log_2 \alpha = [-10 : 2 : 10]$, for each of the three phase encode trajectories in Section 2.4. We reconstructed 24-frame image sequences from 12 'full' frames of data, meaning that each reconstructed image frame is associated with only half of the samples that would be acquired in a full traversal of the PE sampling trajectory.

For all tested values of α, we visually examined the PSF over all 24 frames, and plotted the value of the PSF peak vs frame, as well as the frame to frame change in FWHM of the PSF. The results for PSFs of the Original Trajectory are shown in Figure 6. The top portion

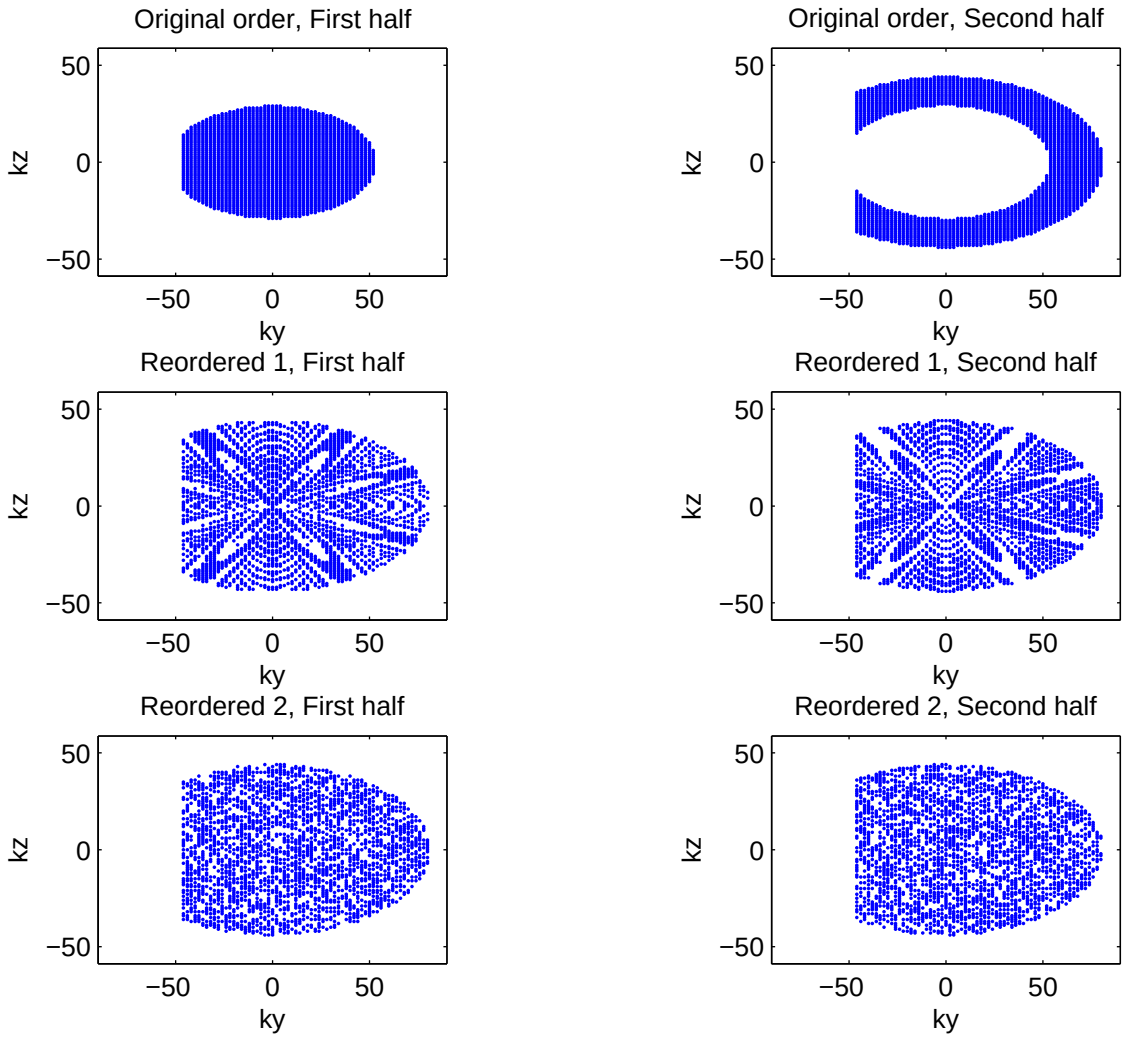

Figure 5: PE locations sampled in the first and second half of a "full" frame acquisition. Sample locations acquired during the first half of acquisition are shown in the left column and those acquired during the second half are shown on the right. The top row shows half frame sample locations from the Original Trajectory, the middle row shows those from Reordered Trajectory 1, and the bottom row shows results from Reordered Trajectory 2.

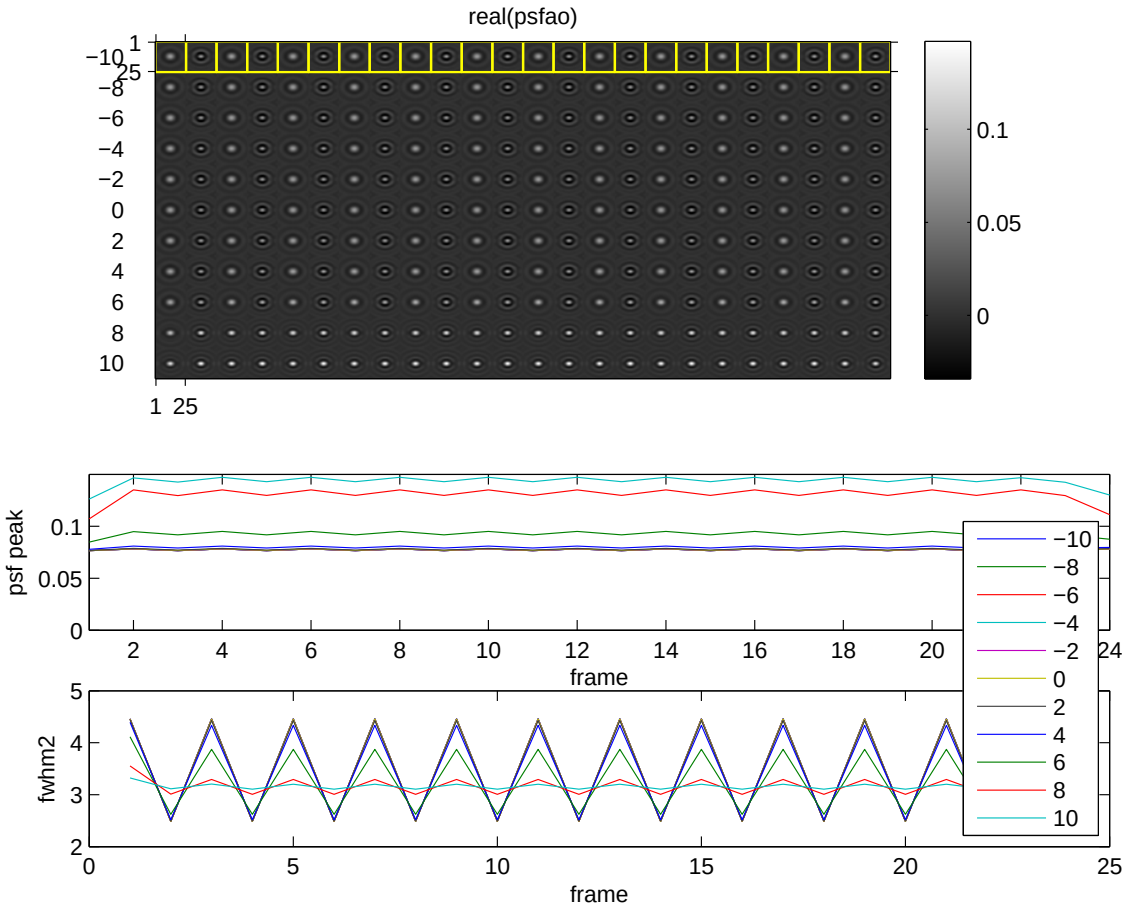

Figure 6: PSF features as a function of α for the Original Trajectory with 24-frame TRUIR reconstruction. The top figure shows the PSF over 24 frames (along the x-axis) for various values of α (y-axis). The middle and bottom plots are of the peak PSF value at each of the 24 frames, and (angularly averaged) FWHM of the PSF at each frame, respectively. Each value of α is represented by a different colored line.

of the figure shows the PSF at each of the 24 reconstructed frames (along the x-axis) for each of the tested values of α (along the y-axis). Here we clearly see that for $\log_2 \alpha$ = -10, the PSF at every even frame looks quite different from the PSFs in the odd frames. For the Original Trajectory, all of the odd frames are associated with the low-frequency half of the PE samples, and all of the even frames are associated with the high-frequency samples in the acquisition. Therefore, the odd and even image frames initially contain complementary information (based on the data-fidelity term), and without sufficient temporal regularization this information is not adequately shared between frames. Thus, for $\log_2 \alpha$ = -10 the PSFs in the odd frames are from only low-frequency samples and appear rather blurred, while the PSFs in the even frames are from only high-frequency samples, which is reflected in the reduced energy and visible sharp edges in the even frames. When we increase $\log_2 \alpha$ to 8 or 10, we start to see the effect of the temporal regularizer across the PSFs of all 24 frames. There is less variability between PSFs in adjacent frames with $\log_2 \alpha = 8$ than $\log_2 \alpha = 6$, and the interframe variability is smaller yet with $\log_2 \alpha = 10$, i.e., the reconstructed PSF is getting closer to the true static impulse.

In an attempt to quantify these qualitative observations, we looked at how the magnitude of the PSF peak changes from frame to frame, for the range of α values. This is the middle plot of Figure 6, where each value of α is represented by a different colored line. Interestingly, we found that the magnitude of the PSF peak changes very little from frame to frame, regardless of the value of α.

As a second attempt to quantify our qualitative observations of clear variability between adjacent image frames, we looked at the change in FWHM from frame to frame, which appears in the bottom plot of Figure 6. Here we see a clear distinction in interframe FWHM variability between α values that resulted in qualitatively bad and good looking PSFs. Values of α whose PSFs show distinct differences between odd and even frames have high interframe FWHM variability. For all tested $\log_2 \alpha$ values less than 6, the FWHM for even frames was about 2.5 pixels, while the FWHM for odd frames was almost twice that, at about 4.5 pixels. However, for $\log_2 \alpha = 8$ and 10, which we have observed result in the best looking PSF sequences, the difference in FWHM between odd and even frames is much smaller, around 0.1-0.2 pixels. These findings suggest that looking at the interframe variability of the FWHM could be useful in choosing a good value for α. A temporal regularization parameter that is sufficient to reduce the interframe FWHM variability of a static PSF may also be sufficient to support adequate sharing of information in reconstructed image sequences of dynamic objects.

Figure 7 shows the PSF images, PSF peak and FWHM over 24 frames for data acquired using Reordered Trajectory 1. The results for both Reordered Trajectories are largely similar, and the following observations hold for both. Because the samples in the Reordered Trajectories are more evenly distributed in k-space over time, we do not see any strong visible differences between PSFs of even and odd frames, even for the smallest tested temporal regularization parameter value of $\log_2 \alpha$ = -10. In fact, visual inspection doesn't show a significant difference in the PSF over 24 frames for $\log_2 \alpha$ = -10 compared to the PSF for $\log_2 \alpha = 10$. Furthermore, the PSFs for the reordered trajectories with any of the tested values for α look visually superior to the best PSF for the Original Trajectory. For the Reordered Trajectories,

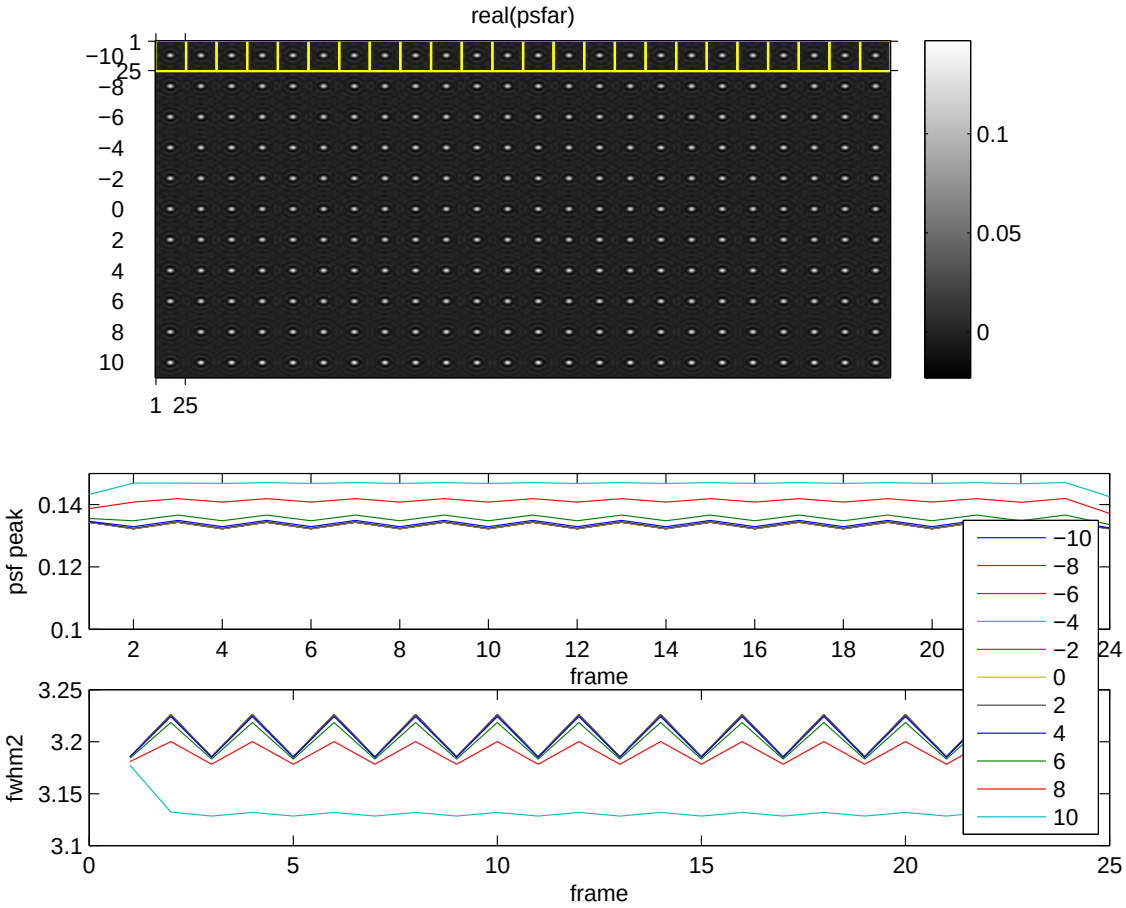

Figure 7: PSF features as a function of α for Reordered Trajectory 1 with 24-frame TRUIR reconstruction. The top figure shows the PSF over 24 frames (along the x-axis) for various values of α (y-axis). The middle and bottom plots are of the peak PSF value at each of the 24 frames, and (angularly averaged) FWHM of the PSF at each frame, respectively. Each value of α is represented by a different colored line.

the difference in FWHM between frames does not show much dependence on α, at least within the range of αs included in this simulation. The maximum change in FWHM The interframe variability in FWHM for reconstructions from the Reordered Trajectories does not provide any indication for choosing one value of α over another, as it did for the Original Trajectory. This result suggests that reconstructions of samples acquired using Reordered Trajectory 1 or Reordered Trajectory 2 may be more robust to the choice of the temporal regularization parameter, α, than are reconstructions of samples acquired using the Original Trajectory.

We examined one other measure of the effect of α on the static impulse response that may aid in regularization parameter selection: the energy contained in the tails of the PSF. For each PE ordering, we computed the energy in the PSF tails, for frame 12 and frame 13 of a 24-frame reconstruction (again reconstructed from 12 'full' frames of data). We defined the

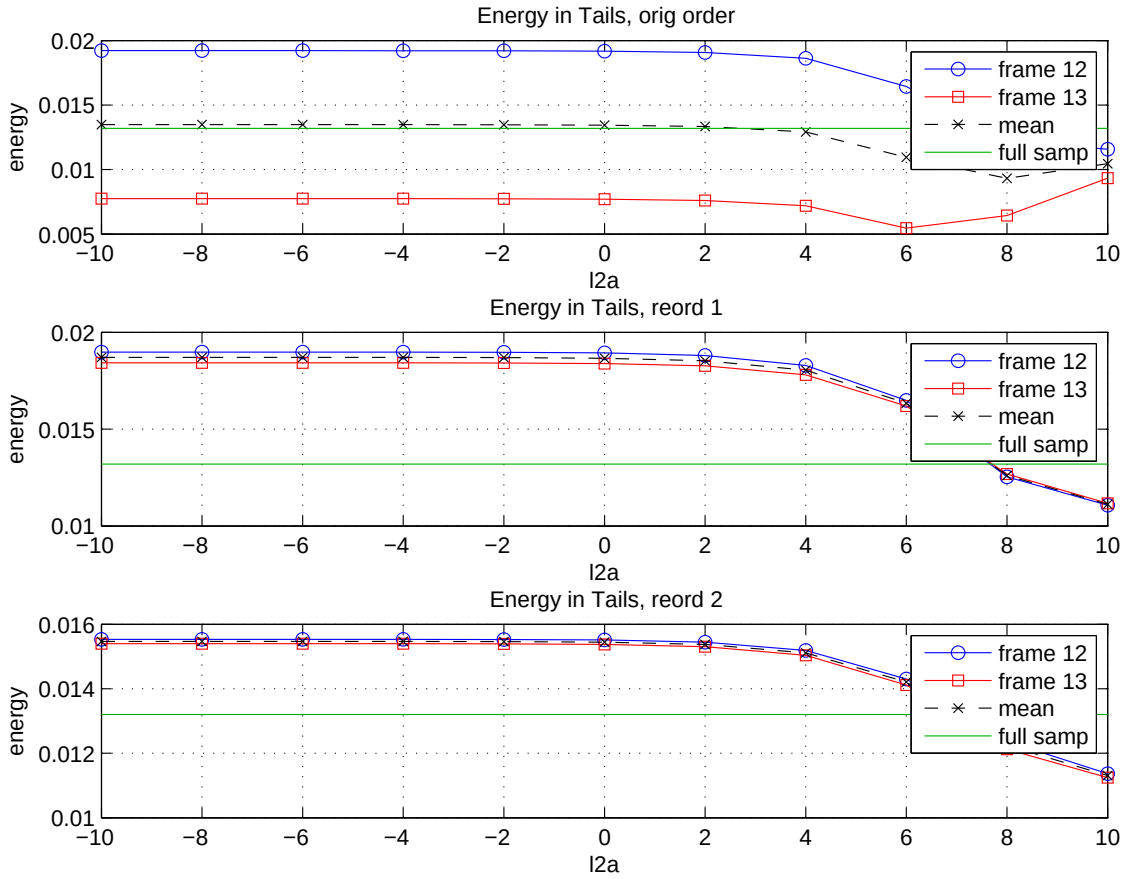

Figure 8: PSF tail energy vs α.

tails to consist of any signal located outside of a ry x rz rectangle, centered at the location of the impulse, where the dimensions of the rectangle were chosen to be equal to 3 FWHMs of the PSF reconstructed from a full frame's worth of samples. The results are shown as a function of α in Figure 8. For each trajectory, the tail energy in the 12th and 13th frames is shown, as well as the mean tail energy of those frames, and the tail energy that exists in a single fully sampled frame (i.e., includes all 4766 samples from a full traversal of one of our PE trajectories).

As we saw with the FWHM comparison, for the Original Trajectory the energy in the tails in even frames is quite different than the energy in the tails in odd frames, for most values of α within the tested range. The energy in the tails for even and odd frames begins to converge around $\log_2 \alpha$ of 8 or 10, which is consistent with our previous findings based on interframe variability of the FWHM. For the Reordered Trajectories, the energy in the tails of the even and odd frames is fairly close for all tested values of α, and is reduced for larger values of α, in the range $\log_2 \alpha = 8$ to 10.

The results of examining the energy in the the PSF tails supports our previous findings that the choice of temporal regularization parameter has a much larger effect on PSFs of

the Original Trajectory than on those from the Reordered Trajectories. Again this suggests relative robustness of the Reordered Trajectories to temporal regularization parameter choice.

The conclusions from our studies on the selection of the temporal regularization parameter for multi-coil TRUIR are as follows. For 24-frame reconstructions of samples acquired according to the Original Trajectory, we need to use a relatively large value for α, in the range of $\log_2 \alpha = 10$, to enforce enough temporal smoothness for adjacent frames to adequately share their complementary information, thereby compensating for the undersampling in each frame. For 24-frame reconstructions of samples acquired using Reordered Trajectory 1 or Reordered Trajectory 2, we examined many measures, but did not find any clear indicators for choosing one α over another. That is, we found all of the PSF features that we investigated to be relatively insensitive to the choice of α (within the range that we tested $\log_2 \alpha = [-10 to 10]$). This is good news, as it suggests a relative robustness to temporal regularization parameter choice for the Reordered Trajectories, which means that we should be able to reconstruct quality image sequences without spending too much time looking for an α that is "just right".

We must also note that because the simulations outlined above used an impulse that is static in time, we were able to find temporal regularization parameter values that were too small, i.e., did not provide enough connectivity between frames, but our simulation results indicate nothing about values that are too large, i.e., provide too much connectivity between frames (since the true object did not vary over time). Examining simulation results of a realistic dynamic phantom will shed further light on the topic of temporal regularization parameter selection, and a subset of these results is presented in Section 2.6.

2.6 DCE-MRI Simulations and Results

In dynamic contrast-enhanced (DCE) MRI, a contrast agent is used to enhance the MR images. The uptake of contrast agent in tissue has been shown to be clinically important in detection and diagnosis of breast cancer, as well as other cancers. The contrast agent is injected into the subject's blood stream and as it travels through the body, it affects the underlying physical mechanisms of MRI and thereby alters the appearance of various tissues in the MR image [8–11]. The enhancement characteristics of tumors differ from those of healthy tissue; enhancement characteristics also differ between healthy and benign lesions. These differences in enhancement arise from differences in vascular permeability as well as differing angiogenic properties [12].

Standard parameters are used to measure the kinetics of DCE-MRI, including the volume transfer constant, K^{trans}, and the rate constant, k_{ep}, [13]. One of the aims of this project was to evaluate the utility of our reconstructed image sequences to provide accurate estimates of these clinically important kinetic parameters.

We simulated DCE-MR breast imaging with a dynamic, bilateral 2D digital phantom, representing a slice through the breast in the sagittal plane. We included 6 lesions, with 3 distinct enhancement patterns: slow, moderate, and rapid enhancement. A small (radius = 2 pixels) and large lesion (radius = 10 pixels) were included for each enhancement pattern.

Our chosen true kinetic parameter values fall within the (wide) range of those reported in the literature [14–19], and correspond with values used by a previous PhD student to

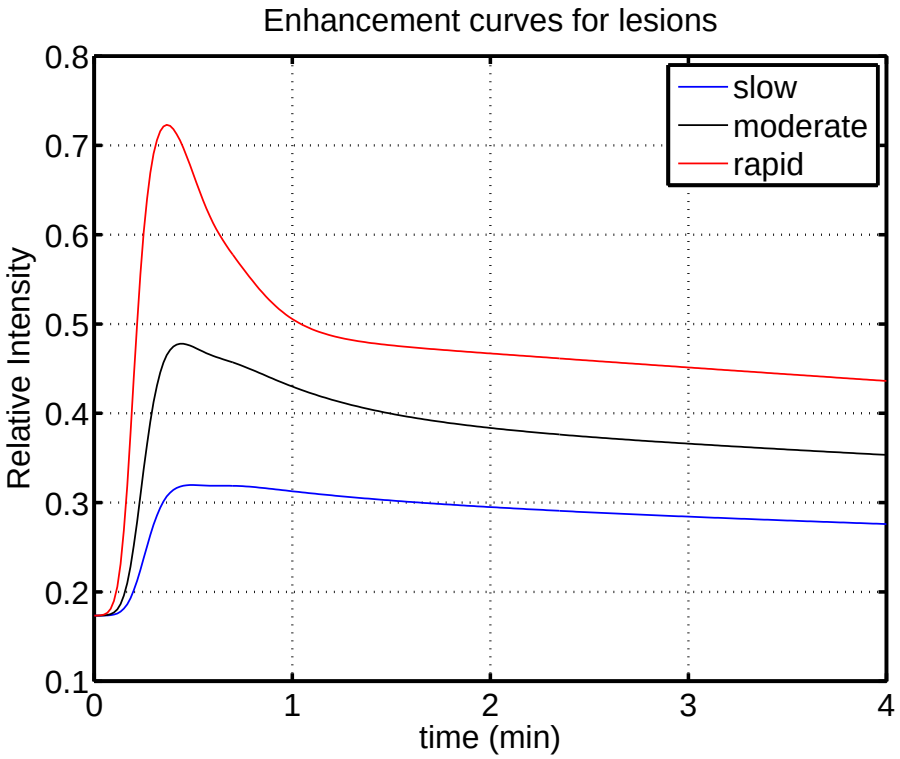

Figure 9: True enhancement curves for the slow, moderate, and rapidly enhancing lesions in our simulated object.

simulate enhancement of breast lesions [20]. The slowly enhancing lesion has $K^{\text{trans}} = 0.2$ min^{-1}, $k_{\text{ep}} = 1.3$ min^{-1}, and $v_{\text{e}} = 0.15$. The moderately enhancing lesion has $K^{\text{trans}} = 0.6$ min^{-1}, $k_{\text{ep}} = 2.0$ min^{-1}, and $v_{\text{e}} = 0.3$, while the rapidly enhancing lesion has $K^{\text{trans}} = 3.0$ min^{-1}, $k_{\text{ep}} = 6.0$ min^{-1}, and $v_{\text{e}} = 0.5$. The "healthy" tissue in our simulations does not exhibit any enhancement. Figure 9 shows the true enhancement patterns for the modeled lesions, and Figure 10 shows the true dynamic object at 1 minute, when the lesions are beginning to show enhancement.

We use the object's true enhancement at each TR to generate the k-space data, one PE location at a time. As in an actual MR scan of a dynamic object, each PE sample in our simulations represents the dynamic object at a different point in time. This was a multi-coil simulation in which we used real sensitivity maps from a 7-coil breast array. We generated three sets of k-space data, according to the three Phase Encode Trajectories discussed in Section 2.4. Each data set consists of 12 full traversals of each PE trajectory, i.e., we generated 12 'full' frames of data.

We reconstructed 12 and 24-frame dynamic image sequences from the simulated data using our proposed TRUIR method, as well as with a more traditional Homodyne+SENSE (HS) reconstruction for comparison [21]. For our TRUIR reconstructions, we tested 3 values for the spatial regularization parameter β ($\log_2 \beta = [-8, 0, 6]$), and 11 values for the temporal

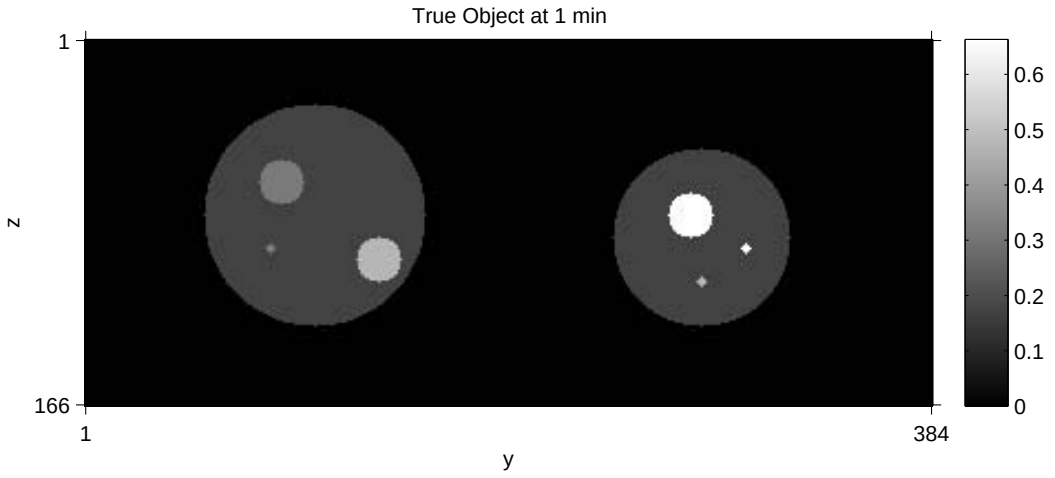

Figure 10: True dynamic object used in our simulations, shown at a single point in time (1 minute).

regularization parameter α ($\log_2 \alpha = [0 : 2 : 20]$), which yields a total of 33 combinations of regularization parameters, and therefore a total of 66 dynamic TRUIR reconstructed image sequences of each data set (33 12-frame reconstructions + 33 24-frame reconstructions).

We found that TRUIR reconstructed image sequences had more accurate temporal dynamics than HS reconstructions, but suffered in spatial resolution, compared to HS reconstructions. TRUIR reconstructed image sequences were better able to capture the lesions' enhancement, than were HS reconstructions. Figure 11 shows the TRUIR enhancement error as a function of the temporal regularization parameter, α. All TRUIR reconstructions represented in this figure use $\log_2 \beta = 6$. The enhancement value shown for each reconstruction is the mean normalized absolute enhancement error, averaged over all 6 lesions and all frames. The enhancement for each lesion is measured at the center pixel of the lesion. The mean enhancement error of a traditional 12-frame HS reconstruction of the Original Trajectory is included for reference, as is the enhancement error of the best HS reconstruction, which was a 24-frame reconstruction of Reordered Trajectory 1.

Figure 11 shows that all TRUIR reconstructions beat even the best HS reconstruction, for a range of values of α. The 24-frame TRUIR reconstruction of the Original Trajectory is the most sensitive to the choice of temporal regularization parameter, giving huge errors for most values of α and only beating the best HS reconstruction for a single value of α ($\log_2 \alpha = 8$). TRUIR reconstructions based on the Reordered Trajectories (12 and 24-frame reconstructions) exhibit more robustness to the choice of temporal regularization parameter, showing good performance for a large range of α values, as does the 12-frame TRUIR reconstruction of the Original Trajectory. All 12-frame TRUIR reconstructions show fairly constant enhancement error for $\log_2 \alpha = 0$ to 8, regardless of trajectory.

The 24-frame TRUIR reconstructions of the reordered trajectories show the overall best performance in terms of enhancement error, with the error minimized with a temporal regularization parameter in the range of $\log_2 \alpha = 6$ to 8. The lowest enhancement error over

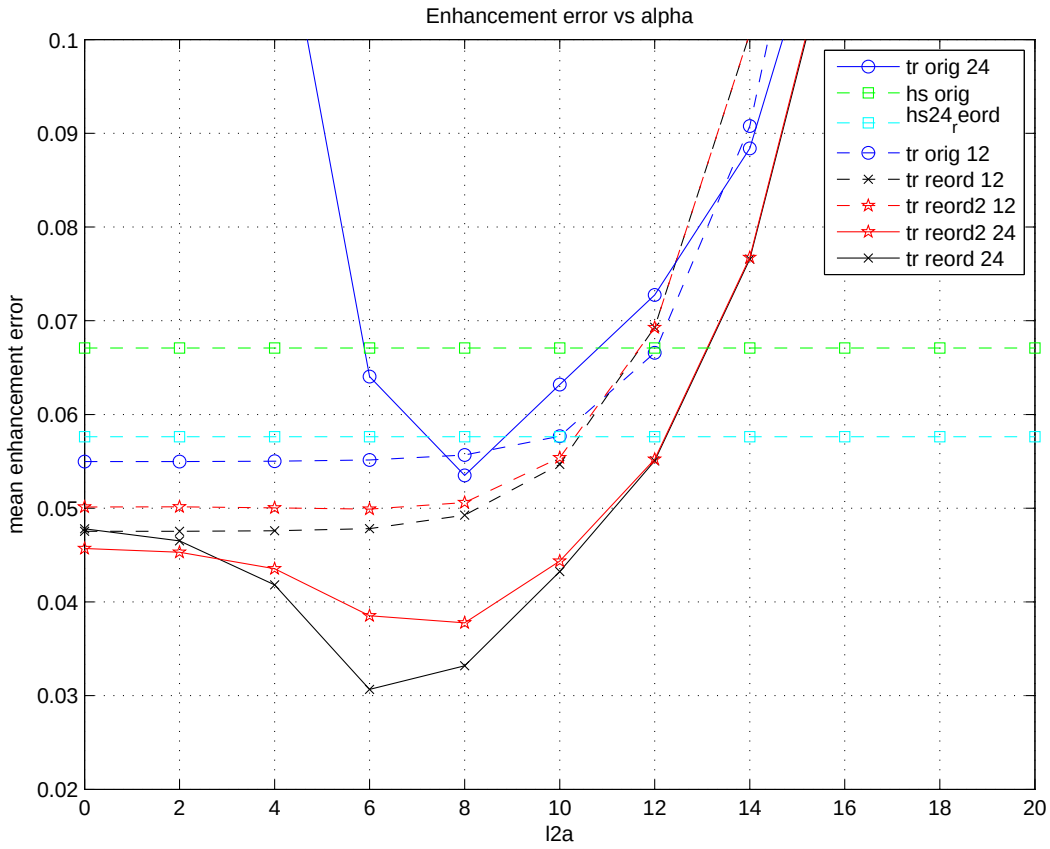

Figure 11: Enhancement error as a function of temporal regularization parameter, α. The x-axis shows the values of $\log_2 \alpha$ ('l2a').

all methods was achieved with a 24-frame TRUIR reconstruction of Reordered Trajectory 1 using a temporal regularization parameter of $\log_2 \alpha = 6$.

While our TRUIR image sequences showed more favorable temporal properties than HS reconstructions, they also showed poorer spatial resolution. Figure 12 shows the small, rapidly enhancing lesion, in the 3rd frame of 12-frame reconstructions of data acquired according to the Original Trajectory. The figure shows the true lesion (A), reconstruction using SENSE only (B), HS (C), TRUIR with very small regularization parameters ($\log_2 \alpha = 0$ and $\log_2 \beta = -8$) (D), and TRUIR with $\log_2 \alpha = 6$ and $\log_2 \beta = 6$ (E), along with the normalized absolute error of each reconstruction. We included a TRUIR reconstruction with the small regularization parameters (D) to verify that the increased spatial blur seen in the TRUIR reconstructions is not due to oversmoothing, i.e., using too large regularization parameters.

One can see that the HS reconstruction (C), has less spatial blur in the y-direction (x-axis) than both the SENSE-only (B) and TRUIR reconstructions (D-E). This can also be seen in Figure 13, which shows profiles through the reconstructed lesions. The fact that the two TRUIR reconstructed image frames look almost identical confirms that the spatial blur we see in TRUIR is not a result of using overly large regularization parameters, since the TRUIR reconstruction in (D) used the smallest regularization parameters within the range that we tested.

Because our TRUIR reconstructions have similar spatial resolution to the SENSE-only reconstruction, we can conclude that the superior spatial resolution of HS reconstruction is attributable to the homodyne part of the reconstruction algorithm (and not the SENSE part). The shape of the HS y-profile in Figure 13 also reflects the reduced spatial blur in y.

Recall that all of our simulated trajectories are partial Fourier acquisitions, meaning the number of high frequency measurements is reduced by half in comparison to a traditional symmetric full Fourier acquisition. It is this reduction in high frequency data that results in reduced spatial resolution for our TRUIR reconstructions, in comparison to HS reconstructions. One of the first steps in homodyning (and HS reconstruction) is to run the partial Fourier data through a high pass filter that doubles the high frequencies, which sort of "makes up" for the other half of high frequency measurements that are missing in a partial Fourier acquisition. Our current TRUIR formulation includes nothing akin to this. Our data fidelity term fits the image sequence to the measured data as is - there is no initial doubling of high frequency components, despite the partial Fourier acquisition. Neither does our TRUIR formulation enforce a smooth phase assumption, which is also a key feature of homodyne reconstruction. Adjusting the TRUIR formulation to include some means of accounting for the reduced high frequency data in partial Fourier acquisitions will be an important area of future work. We believe that adding this adjustment will enable TRUIR reconstructions to approach or match the spatial resolution seen in HS reconstructions.

We computed the kinetic parameters K^{trans}, k_{ep}, and v_{e} for each lesion in each reconstructed image sequence, and compared these estimated values to the true kinetic parameter values. Kinetic parameters were estimated based on the measured enhancement curve at the center of each lesion [8–11, 13, 22]. Figure 14 shows the error in the estimated K^{trans}, which is representative of what we saw for all three kinetic parameters. Figure 14 shows the K^{trans} esti-

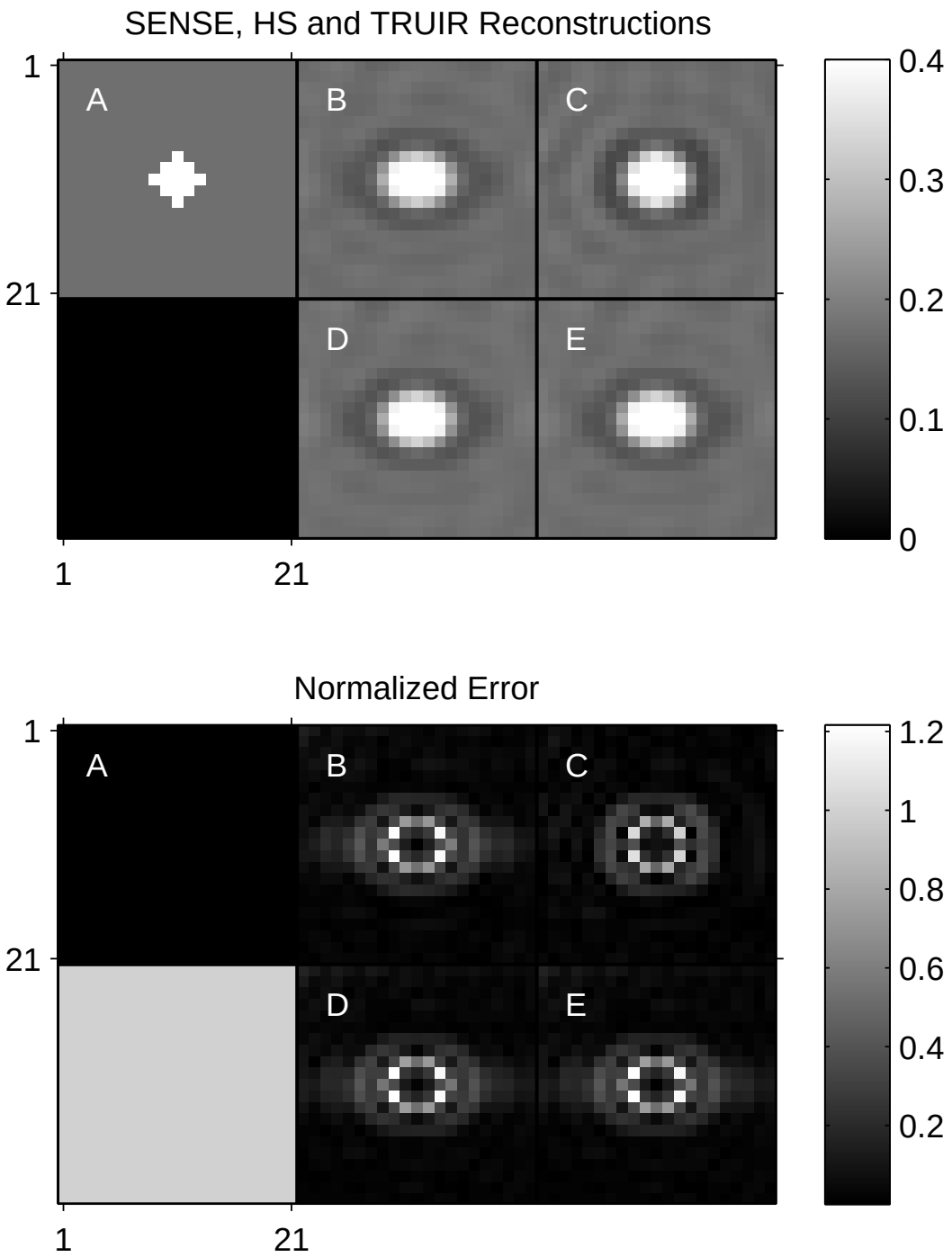

Figure 12: SENSE-only, HS, and TRUIR 12-frame reconstructions of the small, rapidly enhancing lesion. Reconstructions (top), and the normalized absolute error of each reconstruction (bottom). Frame 3 is shown. A: true, B: SENSE only, C: HS, D: TRUIR with $\log_2 \alpha = 0$, $\log_2 \beta = -8$, E: TRUIR with $\log_2 \alpha = 6$, $\log_2 \beta = 6$, H: .

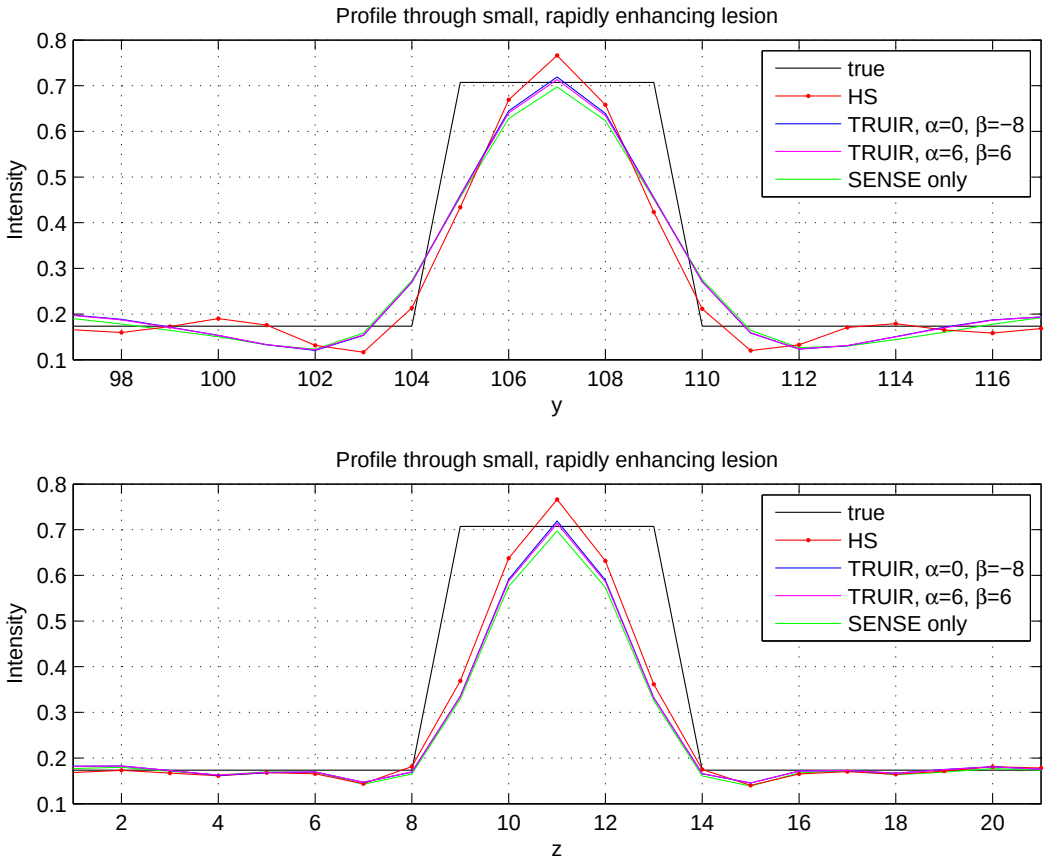

Figure 13: Profiles through SENSE, HS, and TRUIR reconstructions of the small, rapidly enhancing lesion shown in Fig. 12. Profile in the y-direction is shown in the top plot and profile in the z-direction is shown in the bottom one.

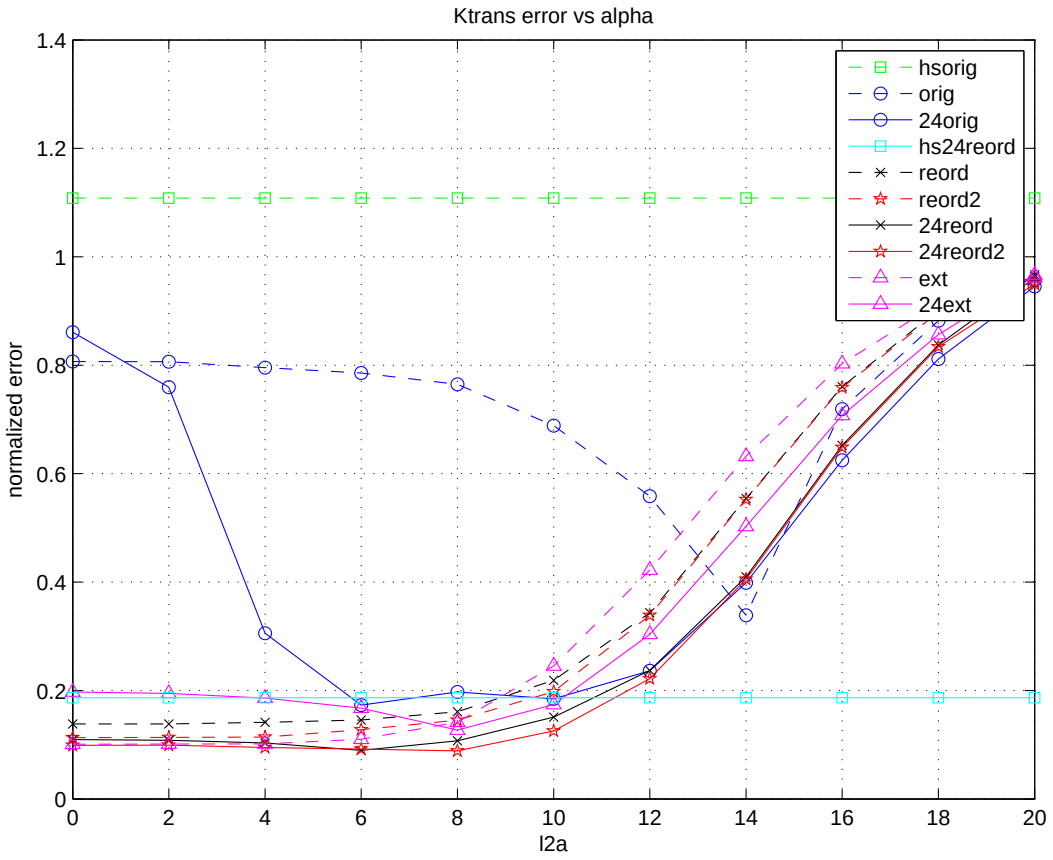

Figure 14: K^{trans} estimation error as a function of α. Error shown for each reconstruction is the mean normalized absolute error of the K^{trans} estimate at the lesion centers, averaged over all lesions.

mation error for for TRUIR reconstructed image sequences as a function of α. All represented TRUIR reconstructions used $\log_2 \beta = 6$. The error shown in the figure is the mean normalized absolute error, averaged over the 6 lesions in each reconstructed image sequence. The figure also includes K^{trans} estimation error calculated from a traditional 12-frame HS reconstruction of the Original Trajectory, for reference. The best HS K^{trans} estimate is included as well. As with the enhancement error, the lowest error in kinetic parameter estimation over all HS reconstructions was achieved with a 24-frame HS reconstruction of Reordered Trajectory 1. Represented results are from TRUIR reconstructions unless otherwise indicated in the legend. Similarly, 24-frame reconstructions are indicated in the legend, and all others are 12-frame reconstructions. The legend entry 'reord' refers to Reordered Trajectory 1.

In Figure 14, we see that all of the presented TRUIR reconstructions result in large improvements in K^{trans} estimates, compared to the traditional 12-frame HS reconstruction of the Original Trajectory. Additionally, a variety of TRUIR reconstructions outperform even the best HS reconstruction in estimating each of the three kinetic parameters. The reconstructions based on the Reordered Trajectories generally provide better kinetic parameter

estimates than reconstructions of the Original Trajectory, and 24-frame reconstructions (solid lines) result in better kinetic parameter estimates than their associated 12-frame reconstructions (dashed lines). As with enhancement error, using a temporal regularization parameter of $\log_2 \alpha <= 8$ generally provides the best estimates of the kinetic parameters. For $\log_2 \alpha < 8$, all 3 kinetic parameters had fairly constant error within each Reordered Trajectory's TRUIR reconstruction, meaning that the Reordered Trajectories are more robust to choice of temporal regularization parameter than the Original Trajectory. Using our proposed TRUIR method, reordered trajectories and higher frame-rate reconstructions, we were able to reduce the estimation error for all three kinetic parameters, compared to the traditional 12-frame HS reconstruction of the Original Trajectory.

2.7 Summary of Results

The main results of our simulation study can be summarized as follows:

- Our proposed Reordered Trajectories 1 and 2 are more suitable for reconstructing dynamic image sequences with an increased frame rate, compared to the Original Trajectory currently in use.

- Choosing the right value for the temporal regularization parameter, α, is very important when reconstructing data from highly ordered, poorly distributed sample trajectories, such as the Original Trajectory, at higher frame rates.

- Our Reordered Trajectories are more robust to the choice of α than the Original Trajectory. Both Reordered Trajectories produced TRUIR image sequences with good temporal resolution and kinetic parameter estimates, over a wide range of temporal regularization parameter values.

- TRUIR reconstructions offer better temporal resolution than even the best HS reconstruction. In particular, 24-frame TRUIR reconstructions of data acquired according to Reordered Trajectory 1 or Reordered Trajectory 2 showed the best overall temporal resolution (for $\log_2 \alpha < 8$), compared to all other reconstructed image sequences, and also resulted in the best kinetic parameter estimates.

- TRUIR reconstructions of the partial Fourier data in this study exhibited poorer spatial resolution properties than HS reconstructions. The HS reconstruction method is designed for reconstruction of partial Fourier data, and includes measures that address the asymmetry of the data, such as doubling of high frequency components and utilizing a smooth phase assumption. Our current TRUIR formulation does not include any such compensation measures for partial Fourier acquisitions. We believe that modification of the TRUIR formulation to better accommodate partial Fourier data will improve the spatial resolution of TRUIR reconstructed image sequences, and this is an important area of future work. Additionally, use of edge preserving regularization will also improve spatial resolution of TRUIR images.

3 Key Research and Training Accomplishments

- Developed and implemented dynamic MR image reconstruction algorithms that are based on explicit temporal models in object space.
- Extended the algorithms to incorporate parallel imaging techniques.
- Algorithm acceleration. Decreased computation time by exploiting Toeplitz matrices in our reconstruction.
- Investigated selection of algorithms' regularization parameters based on desired spatial and temporal resolution.
- Established two new 2D phase encode sampling strategies that are well-suited for reconstructing at increased frame rates, and which also show relative robustness to choice of temporal regularization parameter.
- Implemented realistic simulations using mathematical models that relate enhancements in MR images to the underlying physiological behavior of both healthy and diseased tissues.
- TRUIR reconstructed image sequences provided more accurate enhancement curves as well as more accurate estimates of kinetic parameters, compared to traditional reconstructions, in our studies.

4 Reportable Outcomes

- Created new data objects to assist in TRUIR reconstruction. Added many tools and functions to code base, for use by current and future students and researchers.
- PI successfully completed the qualifying examination and achieved candidacy during this grant period.
- Applied for and awarded NIH grant 1P01 CA87634-06A2, Project 3: Image reconstruction methods for dynamic contrast-enhanced (DCE) MRI of breast cancer.
- PI completed her dissertation research during this grant period, and completed her PhD defense within a month of the end of the funding period.

5 Persons Receiving Pay

The following people received pay from this research effort: Kimberly Khalsa.

6 Publications

Although no papers were published during the grant period, future publications based on the work completed as a result of this grant are in progress.

7 Conclusion

This research project presents an object-domain model for image reconstruction in dynamic MRI, which we refer to as TRUIR: Temporal Regularization Use in Image Reconstruction. Our reconstruction model is formulated as penalized likelihood estimator that explicitly includes a temporal smoothness assumption in object space. TRUIR is therefore well-suited for MR imaging of dynamic objects that vary smoothly in time, such as the objects of interest in dynamic contrast-enhanced MRI. We extended our TRUIR model to incorporate parallel imaging, and also accelerated TRUIR reconstructions by utilizing Toeplitz matrices.

We explored various aspects of the proposed TRUIR method including selection of spatial and temporal regularization parameters, flexibility for increased frame rate reconstruction, and the effect of different phase encode acquisition patterns on TRUIR reconstructions.

As discussed in Section 2.5, we explored TRUIR's resolution properties through evaluation of a local impulse response, and its dependence on the chosen regularization parameters. Our DCE-MRI simulation results also included analysis of spatial and temporal resolution properties, and resolution effects of regularization parameter choice.

We developed two new phase encode sampling trajectories that are based on reordering of sample locations from a current sampling scheme in use for DCE-MRI studies. Our Reordered Trajectories are designed to distribute sampling of low and high frequency locations more uniformly in time. These trajectories offer significantly more flexibility for reconstructing at higher frame rates, and reconstructions of our Reordered Trajectories were also relatively robust to regularization parameter choice, especially when compared to the current trajectory in use.

In evaluating our proposed TRUIR method, we focus on the application of DCE-MRI in the characterization and assessment of breast cancer. We designed a multi-coil simulation study that models dynamic contrast agent uptake in the breast with 6 representative lesions. We compared TRUIR reconstructions to a more traditional frame-by-frame Homodyne + SENSE reconstruction, for a variety of acquired trajectories and reconstructed frame rates. We found that TRUIR provides improved temporal dynamics in the reconstructed dynamic image sequence, compared to the traditional frame-by-frame reconstruction, and that TRUIR achieved the best temporal dynamics when using samples from the Reordered Trajectories and reconstructing at an increased frame rate. TRUIR reconstructions showed improved lesion enhancement curves, and resulted in better estimates of the kinetic parameters K^{trans} k_{ep}, and v_{e}. Our DCE-MRI simulation confirmed our earlier assessment that the Reordered Trajectories are more robust to reconstructing at higher frame rates than the current clinical trajectory, and are also more robust to the choice of the temporal regularization parameter.

Our simulation results also showed the negative result that TRUIR reconstructions ex-

hibited worse spatial resolution than the frame-by-frame Homodyne+SENSE method. We attribute this reduction in spatial resolution to the partial Fourier nature of the PE sampling schemes in this study. Unlike HS reconstruction, our current TRUIR formulation does not include any compensation measures for partial Fourier data. We believe that modification of the TRUIR formulation to better accommodate partial Fourier acquisitions will improve spatial resolution and is an important area of future work.

Future validation of TRUIR with a dynamic phantom study is necessary, as is eventual validation with a human studies. Once the spatial resolution issue has been resolved, and the effectiveness of TRUIR to improve DCE-MR image sequences has been sufficiently established through human studies, TRUIR could be ready for clinical use.

The overall goal of this project was to develop, implement, and evaluate methods for improving image quality in dynamic MR imaging. While our methods may have several potential applications, we focused on areas related to breast cancer. DCE-MRI has been shown to be effective in detection and diagnosis of breast cancer, and is additionally being investigated as a method of early prediction of tumor response to neoadjuvant chemotherapy. Our goal is to provide clinicians with more accurate dynamic MR image sequences, created using our proposed TRUIR reconstruction technique. These improved image sequences will aid in the detection and diagnosis of breast lesions, as well as assist clinicians in evaluating a tumor's initial response to chemotherapy, and thus predict its response (or lack thereof) to an entire course of chemotherapy treatment. For those patients whose tumors are determined to be non-responsive early in the chemotherapy treatment, this mode of therapy could be discontinued. This would save huge amounts to time, emotional strain, and physical distress for these patients, as well as time and money for health care providers.

References

[1] D. K. Sodickson and W. J. Manning, "Simultaneous acquisition of spatial harmonics (SMASH): Fast imaging with radiofrequency coil arrays," *Mag. Res. Med.*, vol. 38, no. 4, pp. 591–603, Oct. 1997.

[2] K. P. Pruessmann, M. Weiger, M. B. Scheidegger, and P. Boesiger, "SENSE: sensitivity encoding for fast MRI," *Mag. Res. Med.*, vol. 42, no. 5, pp. 952–62, Nov. 1999.

[3] M. Bydder, J. Perthen, and J. Du, "Optimization of sensitivity encoding with arbitrary k-space trajectories," *Mag. Res. Im.*, vol. 25, no. 8, pp. 1123–9, Oct. 2007.

[4] R. H. Chan and M. K. Ng, "Conjugate gradient methods for Toeplitz systems," *SIAM Review*, vol. 38, no. 3, pp. 427–82, Sept. 1996.

[5] J. A. Fessler, S. Lee, V. T. Olafsson, H. R. Shi, and D. C. Noll, "Toeplitz-based iterative image reconstruction for MRI with correction for magnetic field inhomogeneity," *IEEE Trans. Sig. Proc.*, vol. 53, no. 9, pp. 3393–402, Sept. 2005.

[6] K. A. Khalsa and J. A. Fessler, "Resolution properties in regularized dynamic MRI reconstruction," in *Proc. IEEE Intl. Symp. Biomed. Imag.*, 2007, pp. 456–9.

[7] J. A. Fessler and W. L. Rogers, "Spatial resolution properties of penalized-likelihood image reconstruction methods: Space-invariant tomographs," *IEEE Trans. Im. Proc.*, vol. 5, no. 9, pp. 1346–58, Sept. 1996.

[8] E. M. Haacke, R. W. Brown, M. R. Thompson, and R. Venkatesan, *Magnetic resonance imaging: Physical principles and sequence design*, Wiley, New York, 1999.

[9] P. S. Tofts and A. G. Kermode, "Measurement of the blood-brain barrier permeability and leakage space using dynamic MR imaging. 1. Fundamental concepts," *Mag. Res. Med.*, vol. 17, no. 2, pp. 357–67, Feb. 1991.

[10] M. Sasaki, E. Shibata, Y. Kanbara, and S. Ehara, "Enhancement effects and relaxivities of gadolinium-DTPA at 1.5 versus 3 Tesla: A phantom study," *Magnetic Resonance in Medical Sciences*, vol. 4, no. 3, pp. 145–9, 2005.

[11] R. Rakow-Penner, B. Daniel, H. Yu, A. Sawyer-Glover, and G. H. Glover, "Relaxation times of breast tissue at 1.5T and 3T measured using IDEAL," *J. Mag. Res. Im.*, vol. 23, no. 1, pp. 87–91, Jan. 2006.

[12] M. V. Knopp, E. Weiss, H. P. Sinn, J. Mattern, H. Junkermann, J. Radeleff, A. Magener, G. Brix, S. Delorme, I. Zuna, and G. . Kaick, "Pathophysiologic basis of contrast enhancement in breast tumors," *J. Mag. Res. Im.*, vol. 10, no. 3, pp. 260–6, Sept. 1999.

[13] P. S. Tofts, G. Brix, D. L. Buckley, J. L. Evelhoch, E. Henderson, M. V. Knopp, H. B. Larsson, T. Y. Lee, N. A. Mayr, G. J. Parker, R. E. Port, J. Taylor, and R. M. Weisskoff, "Estimating kinetic parameters from dynamic contrast-enhanced T(1)-weighted MRI of a diffusable tracer: standardized quantities and symbols," *J. Mag. Res. Im.*, vol. 10, no. 3, pp. 223–32, Sept. 1999.

[14] J. Veltman, M. Stoutjesdijk, R. Mann, H. J. Huisman, J. O. Barentsz, J. G. Blickman, and C. Boetes, "Contrast-enhanced magnetic resonance imaging of the breast: the value of pharmacokinetic parameters derived from fast dynamic imaging during initial enhancement in classifying lesions," *Eur. Radiol.*, vol. 18, no. 6, pp. 1123–1133, Feb. 2008.

[15] P-A. Eliat, V. Dedieu, C. Bertino, V. Boute, J. Lacroix, J-M. Constans, B. . Korvin, C. Vincent, C. Bailly, F. Joffre, J. . Certaines, and D. Vincensini, "Magnetic resonance imaging contrast-enhanced relaxometry of breast tumors: an MRI multicenter investigation concerning 100 patients," *Mag. Res. Im.*, vol. 22, no. 4, pp. 475–81, May 2004.

[16] M. D. Pickles, M. Lowry, D. J. Manton, P. Gibbs, and L. W. Turnbull, "Role of dynamic contrast enhanced mri in monitoring early response of locally advanced breast cancer to neoadjuvant chemotherapy," *Breast Cancer Res Treat*, vol. 91, pp. 1–10, 2005.

[17] T. E. Yankeelov, M. Lepagea, A. Chakravarthy, E. E. Broome, K. J. Niermann, M. C. Kelley, I. Meszoely, I. A. Mayer, C. R. Herman, K. McManus, R. R. Price, and J. C. Gore, "Integration of quantitative dce-mri and adc mapping to monitor treatment response in human breast cancer: initial results," *Mag. Res. Im.*, vol. 25, no. 1, pp. 1–13, Jan. 2007.

[18] J. Li, Y. Yu, Y. Zhang, S. Bao, C. Wu, X. Wang, J.Li, X. Zhang, and J. Hu, "A clinically feasible method to estimate pharmacokinetic parameters in breast cancer," *Med. Phys.*, vol. 36, no. 8, pp. 3786–3794, Aug. 2009.

[19] A. Thukral, D. M. Thomasson, C. K. Chow, R. Eulate, S. B. Wedam, S. N. Gupta, B. J. Wise, S. M. Steinberg, D. J. Liewehr, P. L. Choyke, and S. M. Swain, "Inammatory breast cancer: Dynamic contrast-enhanced mr in patients receiving bevacizumab- initial experience," *Radiol.*, vol. 244, no. 3, pp. 727–735, Sept. 2007.

[20] S. Krishnan, *K-space acquisition method for dynamic contrast-enhanced MRI: Application to breast tumors*, Ph.D. thesis, Univ. of Michigan, Ann Arbor, MI, 48109-2122, Ann Arbor, MI, 2004.

[21] K. F. King and L. Angelos, "SENSE with partial Fourier homodyne reconstruction," in *Proc. Intl. Soc. Mag. Res. Med.*, 2000, p. 153.

[22] G. Golub and V. Pereyra, "Separable nonlinear least squares: the variable projection method and its applications," *Inverse Prob.*, vol. 19, no. 2, pp. R1–26, Apr. 2003.